



LAWRENCE
LIVERMORE
NATIONAL
LABORATORY

Kinetic measurement and prediction of the hydrogen outgassing from the polycrystalline LiH/Li₂O/LiOH system

L. N. Dinh, D. M. Grant, M. A. Schildbach, R. A. Smith, W. J. Siekhaus, B. Balazs, J. H. Leckey, J. Kirkpatrick, W. McLean II

April 11, 2005

Journal of Nuclear Materials

Disclaimer

This document was prepared as an account of work sponsored by an agency of the United States Government. Neither the United States Government nor the University of California nor any of their employees, makes any warranty, express or implied, or assumes any legal liability or responsibility for the accuracy, completeness, or usefulness of any information, apparatus, product, or process disclosed, or represents that its use would not infringe privately owned rights. Reference herein to any specific commercial product, process, or service by trade name, trademark, manufacturer, or otherwise, does not necessarily constitute or imply its endorsement, recommendation, or favoring by the United States Government or the University of California. The views and opinions of authors expressed herein do not necessarily state or reflect those of the United States Government or the University of California, and shall not be used for advertising or product endorsement purposes.

Kinetic measurement and prediction of the hydrogen outgassing from the polycrystalline LiH/Li₂O/LiOH system.

L. N. Dinh¹, D. M. Grant², M. A. Schildbach¹, R. A. Smith³, W. J. Siekhaus¹, B. Balazs¹, J. H. Leckey³, J. R. Kirkpatrick,⁴ W. McLean II¹

¹Lawrence Livermore National Laboratory, Livermore, CA, USA

²Atomic Weapons Establishment, Aldermaston, UK

³BWXT Y-12, Oak Ridge, TN, USA

⁴Oak Ridge National Laboratory, Oak Ridge, TN, USA

ABSTRACT

Due to the exothermic reaction of lithium hydride (LiH) salt with water during transportation and handling, there is always a thin film of lithium hydroxide (LiOH) present on the LiH surface. In dry or vacuum storage, this thin LiOH film slowly decomposes. We have used temperature-programmed reaction/decomposition (TPR) in combination with the isoconversion method of thermal analysis to determine the outgassing kinetics of H₂O from pure LiOH and H₂ and H₂O from this thin LiOH film. H₂ production via the reaction of LiH with LiOH, forming a lithium oxide (Li₂O) interlayer, is thermodynamically favored, with the rate of further reaction limited by diffusion through the Li₂O and the stability of the decomposing LiOH. Lithium hydroxide at the LiOH/vacuum interface also decomposes easily to Li₂O, releasing H₂O which subsequently reacts with LiH in a closed system to form H₂. At the onset of dry decomposition, where H₂ is the predominant product, the activation energy for outgassing from a thin LiOH film is lower than that for bulk LiOH. However, as the reactions at the LiH/Li₂O/LiOH and at the LiOH/vacuum interfaces proceed, the overall activation energy barrier for the outgassing approaches that of bulk LiOH decomposition. The kinetics developed here predicts a hydrogen evolution profile in good agreement with hydrogen release observed during long term isothermal storage.

INTRODUCTION

Lithium hydride (LiH) salt has a high affinity for water. The reaction of hydride with water generates hydrogen gas and heat, the effects of which may be undesirable and pose compatibility or safety issues under certain circumstances. Many different aspects of the reaction of H₂O with LiH to form hydrogen have been investigated in careful detail [1-2]. Even in the absence of a H₂O releasing source, hydrogen generation from within the LiH/Li₂O/LiOH surface layers have been reported [3-5]. There have also been efforts to qualitatively explain and to partially approximate hydrogen outgassing based on the experimental existence of some form of unstable LiOH [4-5]. However, to our knowledge, there is no public record of a complete and quantitative study of the hydrogen outgassing profile from the LiH/Li₂O/LiOH system.

In this report, we present the use of temperature programmed reaction/decomposition (TPR) in the isoconversion mode, in conjunction with field emission scanning electron microscopy (SEM) and atomic force microscopy (AFM) to (1) identify possible hydrogen producing reaction pathways, (2) measure the outgassing kinetics and (3) make kinetic predictions concerning hydrogen outgassing from the polycrystalline LiH/Li₂O/LiOH system in the absence of any external H₂O source.

EXPERIMENTS

The surface roughness of a typical pressed polycrystalline salt sample was probed with a commercial AFM (Digital Nanoscope IV in tapping mode) in ambient air. A Hitachi field emission scanning electron microscope (model S4500) was also employed in the secondary electron mode to obtain images of the LiOH corrosion layer grown on pressed polycrystalline

LiH (by mechanically fracturing a sample of polycrystalline LiH salt in ambient air and examining the fractured surfaces). SEM was also used to examine the morphology of the thin corrosion layer after TPR heating to 550K in vacuum.

Hydrogen outgassing from the LiH/Li₂O/LiOH system was investigated mainly by TPR on 1 mm thick pressed polycrystalline LiH (100 μm to 200 μm grain size) with heating rates in the range of 0.0005 K/s - 0.1 K/s. Our TPR experiments involved two types of salt: fresh and baked salt. Here, fresh salt refers to salt samples that have been polished with 1200 (P-4000) grit silicon carbide sand paper in our air-conditioned laboratory (400Pa -600 Pa of H₂O partial pressure as measured by a Kahn dew-point hygrometer) to remove hydroxide/oxide surface layers and then exposed to room air for 21-30 minutes prior to the introduction into the TPR chamber. The room air exposure described above produced LiOH corrosion layers with a mean thickness of 1.22 μm and an associated standard deviation of 0.11 μm as deduced from the mass spectrometer signals employed in the TPR experiments. Baked salt was fresh salt which had been heated to between 550K and 580K in a vacuum to convert hydroxide into oxide (as verified by the mass spectrometer used in TPR experiments). After cooling down to room temperature under high vacuum, the baked samples were then re-exposed to 3 Pa of H₂O pressure (30 ppm of H₂O) for 2.5 hours. This H₂O re-exposure resulted in the formation of a quantity of LiOH equivalent to an LiOH layer with a mean thickness of 0.28 μm and an associated standard deviation of 0.04 μm as deduced from the mass spectrometer signals employed in the TPR experiments. We also performed TPR on laboratory grade bulk LiOH powder with grain sizes in the range of many tens of micrometers to a few hundreds of micrometers obtained from Fisher Chemicals. Bulk LiOH powder samples were prepared by encapsulating about 45 mg of powder within a 1 cm² square platinum envelope. The envelopes were constructed from 0.025 mm thick

platinum foil. The front face of each envelope was fully perforated to allow gases generated during TPR experiments to freely flow toward the mass spectrometer.

In a typical TPR experiment, the sample was attached to a sample holder by way of mechanical clamps and transferred, through a differentially pumped load lock, into an ultrahigh vacuum (UHV) sample chamber with a base pressure of 10^{-6} Pa. Within the sample chamber, the sample holder sat on a rotatable XYZ manipulator. The sample temperature was measured via a type K thermocouple inserted between the sample's front surface and one of the mounting clamps. Linear heating was achieved by passing current through a tungsten coil located 2 mm behind the sample. The heating rate was computer-controlled. The sample chamber was connected by a 6 mm diameter orifice to a separately pumped detector chamber equipped with a Balzers quadrupole mass spectrometer which was in line of sight of the sample. The base pressure in the detector chamber was usually less than 10^{-7} Pa. During the experiment, the sample was positioned ~ 2 mm from the orifice facing the detector chamber. This arrangement guaranteed that only gases originating from the portion of the sample in line with the 6 mm orifice contributed to the gas flux detected by the quadrupole mass spectrometer.

In order to test the validity and accuracy of kinetic measurements and predictions based on the isoconversion analysis of TPR outgassing spectra, a set of long-term (i.e. > 180 days) isothermal outgassing experiments were undertaken. Our isothermal outgassing experiments involved stored and annealed salt. Stored salt was maintained in an environment with ≤ 10 ppm of H_2O , over an extended period of time, until insertion into previously baked and thoroughly outgassed steel containers equipped with Baratron capacitance gauges and valves for pump-down (by a turbo molecular pump). Annealed salt was stored salt which had been annealed in a dry environment (less than a few ppm of H_2O) at 503 K for 40 hours, cooled down and then re-

exposed to 30 ppm of H₂O for 2-3 hours. Diffuse Reflectance Infrared Fourier Transform spectroscopy (DRIFT) indicated that the LiOH surface thickness was on the order of 0.26 μm for both stored and annealed salt. After pump down, the containers were placed within ovens set at different temperatures. Empty control vessels (no salt inside) served to establish a background outgassing level. At the end of the isothermal experiments, the gas content in each container was analyzed and found to be mostly H₂ (~99% H₂ and ~ 1% trace amounts of N₂ + O₂ + Ar). The H₂ outgassing properties of stored and annealed salt in isothermal experiments (performed at BWXT Y-12 facility in Oak Ridge, Tennessee) will be compared to those predicted from kinetic measurement of fresh and baked salt by TPR experiment (performed at Lawrence Livermore National laboratory in Livermore, California) respectively.

ANALYSIS

The kinetics of the reactions were obtained by analyzing the TPR spectra of similarly prepared samples at different heating rates in accordance with the isoconversion method of thermal analysis as described below.

The rate equation for a solid-state reaction can be written as [6-9]:

$$\frac{d\alpha}{dt} = kf(\alpha) = \nu e^{-\frac{E}{RT}} f(\alpha) \quad (1)$$

where t is time; α is the reacted-fraction (0 to 1); ν is the pre-exponential factor which includes many constants describing the initial state of the sample such as three-dimensional shape factors of initial particles, molecular mass, density, stoichiometry, active surface factors, number of lattice imperfections, and so forth; E is the activation energy for the rate controlling process, R is

the molar gas constant, and $f(\alpha)$ is an analytical function determined by the rate-limiting reaction mechanism. In this equation, $k = \nu e^{-\frac{E}{RT}}$ is the rate constant.

With a heating rate of $\beta = dT / dt$:

$$\frac{d\alpha}{dT} = \left[\frac{\nu}{\beta} f(\alpha) \right] e^{-\frac{E}{RT}} \quad (2)$$

Taking the natural logarithm on both sides of equation (2) and integrating with respect to $d\alpha$ yields:

$$\int_0^{\alpha} \ln \left(\frac{d\alpha}{dT / \beta} \right) d\alpha = -\frac{E}{R} \int_0^{\alpha} \frac{d\alpha}{T} + \int_0^{\alpha} \ln(\nu f(\alpha)) d\alpha \quad (3)$$

At any given α , the second term on the right-hand side of equation (3) is a constant, irrespective of the heating rate β . So, at a chosen value of α , a plot of $\int_0^{\alpha} \ln \left(\frac{d\alpha}{dT / \beta} \right) d\alpha$ against $\int_0^{\alpha} \frac{d\alpha}{T}$ for a set of different heating rates has a slope of $-E/R$. A plot of E vs. α is thus obtained by repeating the above procedure at other α values between 0 and 1 [10]. In practice, due to a poor signal-to-noise ratio near the beginning and the end of most chemical reaction experiments, data outside an α range of 0.1-0.2 to 0.8-0.9 should be discarded.

With $g(\alpha) \equiv \int_0^{\alpha} \frac{d\alpha}{f(\alpha)}$ and for isothermal conditions:

$$g(\alpha) = \left[\nu e^{-\frac{E}{RT}} \right] \int dt = \left[\nu e^{-\frac{E}{RT}} \right] t \quad (4)$$

For non-isothermal conditions with a constant heating rate [11]:

$$g(\alpha) = \frac{\nu}{\beta} \int_0^T e^{-\frac{E}{RT}} dT \approx \frac{\nu}{\beta} \frac{RT^2}{E} e^{-\frac{E}{RT}} \quad (5)$$

The time, t_α , at which a given conversion α is reached at an arbitrary temperature T_o can be approximated from non-isothermal experiments for many processes by equating the $g(\alpha)$ forms above for the isothermal and non-isothermal conditions [12-13]:

$$t_\alpha = \left[\beta e^{-\frac{E_\alpha}{RT_o}} \right]^{-1} \frac{RT_\alpha^2}{E_\alpha} e^{-\frac{E_\alpha}{RT_\alpha}} \quad (6)$$

Here, T_α is the temperature corresponding to a given conversion α at the heating rate of β . E_α is the value of the overall activation energy barrier at that level of conversion. For reactions in which E is not constant but increases with α , using equation (6) is equivalent to setting the kinetic parameters: E , ν and $f(\alpha)$ fixed at $E = E_\alpha$, $\nu = \nu_\alpha$ and $f(\alpha) = f_\alpha$ from $\alpha = 0$ to that particular level of conversion α . Iterating equation (6) over every value of α yields a plot of t_α vs. α . This isoconversion technique of analyzing TPR spectra does not assume any particular rate limiting model and so is suitable for the kinetic measurement and prediction of processes with competing reactions and/or an overall activation energy that varies with the conversion level.

RESULTS & DISCUSSION

A typical AFM image of a polished salt surface is shown in the lower portion of Fig. 1. The units on the lateral scale and vertical scale are 2 μm and 1.5 μm per division, respectively. A line scan across the salt surface topography (upper portion of Fig. 1) reveals a surface roughness on the order of 0.5 μm . When LiOH films grew on these polished pressed polycrystalline LiH surfaces, they inherited a similar surface roughness and therefore had a three-dimensional (3D) topography.

Various morphologies of LiOH films grown on polycrystalline LiH surfaces are shown in Fig. 2. Depending on the LiH substrate facets, LiOH corrosion layers are composed of columnar

structures with an average width on the order of a few hundred nanometers (a), nanometer-scale grains (b), wave like structures (c), and some complex nanometer-scale structures (d). Figs. 2(a)-(d) were obtained after the fractured surfaces of a mechanically fractured pressed polycrystalline LiH sample were exposed to roughly 15 minutes of room air with $\sim 30\%$ relative humidity (~ 951 Pa of H_2O partial pressure) at 296-300 K. The thickness of the LiOH films grown on these surfaces was estimated to be approximately $1.2\ \mu\text{m}$ [14]. Figs. 2(e) and (f) show larger nanometer-scale grains observed on some facets of the fractured surfaces of another mechanically fractured polycrystalline LiH sample after exposure to room air for 40 minutes. The thickness of the LiOH films grown on these surfaces was estimated to be approximately $2\ \mu\text{m}$ [14]. Due to large lattice and volume mismatches between LiH and LiOH [15], the formation of these nanometer-scale structures can be attributed to a stress relief mechanism during the growth of the LiOH layer.

The integrity of the Li_2O layers grown on LiH salt as a result of heating to 550 K in vacuum is presented in Fig. 3. In general, the LiOH films under investigation were less than $1.5\ \mu\text{m}$ thick and retained the majority of their integrity even after TPR heating. However, local spallation [the right portion of Fig. 3(a) and Fig. 3(d)], blistering with subsequent spallation [Fig. 3(b)], and blistering with cracks in the vicinity [Fig. 3(c)] were seen. This is in stark contrast to thick ($\gg 3\ \mu\text{m}$) LiOH corrosion layers which tend to develop a large network of cracks to relieve stress-buildup during growth [4].

In Fig. 4(a), we show the TPR spectrum of a fresh salt sample at a heating rate of $0.0015\ \text{K/s}$. The inset of Fig. 4(a) shows a blown-up portion of the same TPR spectrum in the lower temperature region. The TPR spectrum for the decomposition of bulk LiOH powder at a heating rate of $0.002\ \text{K/s}$ is shown in Fig. 4(b). In comparison with Fig. 4(b), the TPR spectrum in Fig.

4(a) may be considered to have two separate but competing reactions: (1) H₂ formation via the reaction of LiOH with LiH forming Li₂O and the thereafter diffusion of OH⁻ from the LiOH/Li₂O interface through the Li₂O buffer layer to react with the LiH substrate as will be discussed in details later (lower temperature region in the TPR spectra where the H₂O signal is weak); (2) the decomposition of LiOH from the LiOH/vacuum surface inward, generating H₂O and forming Li₂O [4-6]. This component is weak in the lower temperature region but becomes more intense with increasing temperature and is dominant in the high temperature region [associated with a high mass 18 signal intensity seen in Fig. 4(a)]. During TPR, some of the generated H₂O proceeded toward the LiH substrate to react and form H₂ while the rest moved toward the vacuum interface and was detected by the mass spectrometer. In a closed system containing LiH and LiOH, all H₂O generated from LiOH decomposition would rapidly react with LiH to form H₂ [3]. Thus, in the absence of any external H₂O source, LiOH is involved in all aspects of hydrogen outgassing from the LiH/Li₂O/LiOH system. In earlier papers, some of the authors have reported the existence of some form of unstable surface/interface LiOH in addition to the more stable bulk LiOH [4, 6]. In this report the existence of LiOH types, with varying propensities for decomposition, will be more rigorously analyzed.

LiOH reacts with LiH according to:



The heat of formation, ΔH , and Gibbs free energy, ΔG , for this reaction are -20 kJ/mol and -49 kJ/mol at 273 K and reduce to -22 kJ/mol and -91 kJ/mol at 673 K, respectively [16].

Reaction (7) is so favorable (as evidenced by negative ΔH and ΔG values) that a Li₂O buffer is quickly formed in between LiH and LiOH, creating a LiOH/Li₂O/LiH interface [17]. Despite the initial formation of a buffer layer, further reaction is not inhibited, but simply gains a

dependency on diffusion through the Li₂O. Initially, the stress/strain caused by lattice, volume and density mismatches at the LiOH/Li₂O/LiH double junction interface [15] weakens the bonds at that location. Since LiOH is the least thermally stable compound at that junction, the transport of OH⁻ by diffusion from the LiOH/Li₂O interface through the Li₂O interlayer to react with LiH (as depicted in Fig. 5), is possible. At no point is water realized within this diffusive system. The diffusion of OH⁻ species through the Li₂O layer is actually equivalent to an H⁺ ion hopping between successive O₂⁻ ions, with a transition state shown in (b). At the Li₂O/LiH interface the two oppositely charged hydrogen ions combine to generate hydrogen gas (c). An oxide ion shift occurs in order to minimize the energy of the subsequent crystalline void (d). The effective result is the diffusion of OH⁻ through Li₂O. This solid-state diffusion reaction at the LiOH/Li₂O/LiH interface produces one mole of H₂ for the decomposition of every mole of LiOH at the LiOH/Li₂O interface.

Thermal decomposition of LiOH can be described as:



The heat of formation, ΔH, and Gibbs free energy, ΔG, for this reaction are 136 kJ/mol and 97 kJ/mol at 273 K and reduce to 127 kJ/mol and 43 kJ/mol at 673 K, respectively [16]. There are a number of experimental reports on the thermal decomposition of LiOH and the common consensus is that LiOH powder decomposes inwards from the LiOH/vacuum interface, while LiOH films grown on LiH decompose inwards from both the vacuum and substrate interfaces [3, 5, 18].

Out of all possible decomposition sites, interfacial LiOH at the LiOH/Li₂O/LiH double junction interface is the least stable as discussed above and shown in Fig. 4(a). Interface/surface states are also present at the LiOH/vacuum boundary (and possibly to some degree at LiOH grain

surfaces). Surface LiOH states are expected to be thermally unstable in comparison with bulk LiOH. Due to defective and missing crystalline bonding at surface sites, lattice vibrations of surface material are at frequencies different to those of the bulk [19], a phenomenon seen in most solids. In addition, surface and interface species have different chemical reactivities and electronic properties to those of their bulk counterparts [19]. It should therefore be of no surprise to find that LiOH located at the LiOH/thin Li₂O/LiH double junction and LiOH at the LiOH/vacuum interface behave differently, in terms of thermal stability and reactivity, to LiOH in the bulk. During thermal decomposition of LiOH, as the Li₂O front moves far away from the LiH and vacuum interfaces, the activation energy for LiOH decomposition eventually increases to the level of bulk LiOH decomposition. Note that at temperatures below ~ 450K, the TPR mass 18 signal is non-zero and increases with heating temperature [inset of Fig. 4(a)], but is quite minimal compared to that of mass 2. This indicates that the H₂ production reaction at the LiOH/Li₂O/LiH interface and the H₂O production reaction due to thermal decomposition of LiOH grown on polycrystalline LiH are competing processes, with the former one having a smaller thermal barrier in the initial stage of outgassing when the Li₂O interlayer is thin.

In a closed system containing both LiH and LiOH, H₂O generated by thermal decomposition of LiOH rapidly reacts with LiH to form H₂ [3] according to:



From the reaction sequence shown in (8) and (9), two LiOH decomposition events generate one intermediate H₂O molecule which, in turn, produces two H₂ molecules. Overall, there is one mole of H₂ formed for the decomposition of one mole of LiOH. In vacuum device applications involving both LiH and LiOH, the total equivalent hydrogen outgassing flux ($\Gamma_{\text{equiv. hydrogen}}$, in

unit of molecules.m⁻².s⁻¹) can, therefore, be approximated by doubling the mass 18 TPR flux ($\Gamma_{\text{mass 18}}$) and adding the results to the mass 2 TPR flux ($\Gamma_{\text{mass 2}}$):

$$\Gamma_{\text{equiv. hydrogen}} = 2\Gamma_{\text{mass 18}} + \Gamma_{\text{mass 2}} \quad (10)$$

Fig. 6 shows that the equivalent H₂ outgassing spectrum of the sample presented in Fig. 4(a) can be divided into two subcomponents, labeled D3 and R3. D3 and R3 simulated outgassing curves were obtained by regression fitting to equation (1), with $f(\alpha) = [1-(1-\alpha)^{1/3}]^2$ and $f(\alpha) = 1-(1-\alpha)^{1/3}$ respectively [9]. The D3 region represents the 3D solid-state diffusion controlled reaction at the LiOH/Li₂O/LiH interface, with a constant activation energy of 69.9kJ/mol. The solid state diffusion reaction contains a three dimensional aspect, as opposed to 1D, to better describe effects introduced by the surface roughness of the polished salt samples, as shown in the AFM image of Fig. 1. The Li₂O thickness, $x_{\text{Li}_2\text{O}}$, formed at the LiOH/Li₂O/LiH interface can be approximated by:

$$x_{\text{Li}_2\text{O}} = \frac{m_{\text{Li}_2\text{O}}}{\rho_{\text{Li}_2\text{O}}} \int \frac{\Gamma_{\text{equiv. hydrogen}}}{\beta} dT \quad (11)$$

where $m_{\text{Li}_2\text{O}}$ (4.98×10^{-26} kg.molecule⁻¹) and $\rho_{\text{Li}_2\text{O}}$ (2013 kg.m⁻³) are the mass of a Li₂O molecule and the density of bulk Li₂O, respectively. Equation (11) suggests a Li₂O interlayer thickness on the order of 0.14 μm due to the solid-state diffusion reaction at the LiOH/Li₂O/LiH interface under the D3 regime. The R3 region represents mainly the thermal decomposition of LiOH with a progressive reaction front moving from the interface/surface inward [9] with a constant activation energy of 93.3 kJ/mol.

The two-part deconvolution of the total equivalent H₂ outgassing (Fig. 6) proves visually helpful in qualitatively identifying the different competing reactions, but assumes constant activation energies in the D3 and R3 regions. There is some degree of arbitrariness in the D3/R3

partitioning. If the assumption of “constant activation energies” was not actualized in the real reactions or if the chosen models for the fit were not ideal, the accuracy of the kinetic prediction from this technique would greatly suffer. A model-independent kinetic analysis, which makes no assumption about constant activation energies for the competing reactions, is much more desirable. For this reason, from this point on, we will present only kinetic measurements and predictions based upon the model-free isoconversion technique, which makes no assumption about the activation energy profile.

In Fig. 7, we show TPR spectra of total equivalent H₂ release rates in units of molecules.m⁻².s⁻¹ from (a) fresh salt at $\beta = 0.0005$ K/s, (b) baked salt at $\beta = 0.005$ K/s, (c) fresh salt at $\beta = 0.025$ K/s, and (d) baked salt at $\beta = 0.025$ K/s. It is seen that the maximum outgassing peak shifted to a higher temperature as the heating rate was increased. This is typical for a thermal process with a positive activation energy barrier. In Fig. 8, we show the plots of

$\int_0^\alpha \ln\left(\frac{d\alpha}{dt}\right)d\alpha$ vs. $\int_0^\alpha \frac{d\alpha}{T}$ for (a) fresh salt and (b) baked salt at α value of 0.3, 0.5, and 0.7. The

plots in Fig. 8 were obtained by taking TPR spectra at different heating rates. Linear regression

through the $\int_0^\alpha \ln\left(\frac{d\alpha}{dt}\right)d\alpha$ vs. $\int_0^\alpha \frac{d\alpha}{T}$ data at different values of α from 0.15 to 0.9 give a plot of E

vs. α for the hydrogen outgassing process from each type of salt. Plots of E vs. α for fresh salt (middle curve) and baked salt (lower curve) are presented in Fig. 9, together with the activation energy plot for LiOH decomposition obtained from bulk LiOH powder TPR experiments (top curve). The outgassing process from thin LiOH films grown on LiH is seen, here, as a complicated process involving competing reactions with an overall activation energy barrier that increases with reacted-fraction, α . The activation energy barrier for hydrogen outgassing from baked salt with an equivalent LiOH layer thickness of ~ 0.28 μm is observed to be much lower,

and have a different shape, to that of fresh salt with a mean LiOH layer thickness of 1.22 μm . This can be understood by the following. Vacuum baking of the LiH/LiOH system at high temperature converts LiOH into Li_2O with the formation of local spallations and cracks within the Li_2O region to relieve stress [6-8]. Upon subsequent low H_2O exposure for 2.5 hours, only a small population of Li_2O (more abundantly near surfaces and defect locations) is converted back to LiOH. The ratio of interface/surface LiOH to bulk LiOH is certainly much higher in systems baked and re-exposed to low H_2O levels, hence the inherent lower activation energy barrier for the decomposition of LiOH formed on baked salt compared to fresh salt. Similarly, the activation energy barrier for hydrogen outgassing from fresh salt is seen to progressively increase with α and is expected to approach that of bulk LiOH powder decomposition for thicker, multi-micron, LiOH corrosion layers. This is easily seen if the activation energy barrier for outgassing is plotted vs. the equivalent LiOH decomposition thickness for fresh salt [Fig. 10], where the LiOH decomposition thickness, x_{LiOH} , is derived according to:

$$x_{\text{LiOH}} = \frac{m_{\text{LiOH}}}{\rho_{\text{LiOH}}} \int \frac{\Gamma_{\text{equiv. hydrogen}}}{\beta} dT \quad (12)$$

In equation (12), m_{LiOH} ($3.99 \times 10^{-26} \text{ kg.molecule}^{-1}$) and ρ_{LiOH} (1460 kg.m^{-3}) are the mass of a LiOH molecule and the density of bulk LiOH, respectively. During moisture bombardment, most of the LiOH formed early in the process is surface/interface LiOH. However, there is a limit to the number of sites available to form surface/interface LiOH. Once these sites are used up, the remaining LiOH creation is almost exclusively bulk. As a result, one expects an inverse relationship between the activation energy barrier for hydrogen outgassing in the LiH/ Li_2O /LiOH system and the LiOH corrosion layer thickness. Indeed, this is the reason why the H_2O peak from bulk LiOH powder decomposition TPR spectrum in Fig. 4(b) is shifted by \sim

80K to a higher temperature in comparison with the H₂O peak from the fresh salt TPR spectrum in Fig. 4(a), given their very small difference in heating rate.

A comparison between experimental isothermal hydrogen outgassing from stored salt, with a total geometrical surface area of 0.0190 m², and an outgassing prediction based on the model-free kinetic analysis for fresh salt, with a similar surface area, at 343 K is presented in Fig. 11(a). Figs. 11(b), (c) and (d) show comparisons between experimental isothermal hydrogen outgassing from annealed salt, with a total geometrical surface area of 0.0205 m², and outgassing predictions based on the model-free kinetic analysis for baked salt at 348.7 K, 330.1 K and 315.5 K respectively. The heavy lines indicate experimental isothermal hydrogen outgassing data while the lighter bands are predicted from the isoconversion kinetic analysis of TPR spectra. Despite noticeable scatters in the experimental isothermal outgassing curves, it is recognized that experimental and predicted curves correlate well. Inconsistencies, in particular between (c) and (d) where increased outgassing is seen at the lower temperature, are due to unavoidable sample to sample variations, assembly conditions and instrument response, but are to be expected over long term trials such as these. Given these unavoidable differences in preparation conditions and variations in LiH sample treatment between TPR (Lawrence Livermore National Laboratory, California) and isothermal (BWXT Y-12 laboratory, Tennessee) experiments, the majority of the isothermal data falls within the kinetic prediction bounds and more importantly the curve shapes are well represented, adding additional credence to the reacted-fraction dependent activation energies. Using the methodology presented here, and with the help of equation (6), time dependent kinetic predictions for hydrogen release from the LiH/LiOH system can be made at any temperature and as a function of sample pre-treatment.

CONCLUSIONS

In summary, we have applied the technique of temperature programmed reaction/decomposition in combination with the isoconversion method of thermal analysis to make kinetic predictions for the hydrogen outgassing profile of the polycrystalline LiOH/Li₂O/LiH system. Our kinetic predictions agree well with experimental isothermal outgassing data. In the course of this work, we have found that LiOH, in particular LiOH at the LiOH/thin Li₂O/LiH and LiOH near the LiOH/vacuum interface, is involved in all aspects of hydrogen outgassing and have proposed mechanisms for such a process. Our experimental results reveal that the initial activation energy for outgassing from the thin LiOH film grown on LiH is significantly lower than that for bulk LiOH decomposition, but increases as the reaction proceeds, approaching the bulk LiOH value in multi-micrometer thick films. The methodology presented in this report can be used to generate isothermal hydrogen outgassing predictions for LiH/LiOH under a variety of initial environmental conditions.

ACKNOWLEDGEMENT

This work was performed under the auspices of the U.S. Department of Energy, by the University of California, Lawrence Livermore National Laboratory under contract No. W-7405-ENG-48.

REFERENCES

1. W. D. Machin and F. C. Tompkins, *Trans. Faraday Soc.* **62**, 2205(1966).
2. M. Balooch, L. N. Dinh, D. F. Calef, *J. Nucl. Mater.* **303**, 200 (2002).
3. S. M. Myers, *J. of Appl. Phys.* **45**, 4320, (1974).

4. L. N. Dinh, C. M. Cecala, J. H. Leckey, M. Balooch, J. Nucl. Mater. **295**, 193 (2001).
5. L. N. Dinh, W. McLean II, M. A. Schildbach, J. D. LeMay, W. J. Siekhaus, M. Balooch, J. Nucl. Mater. **317**, 175 (2003).
6. C. H. Bamford, C. H. F. Tipper, *Comprehensive Chemical Kinetics: Reaction in the Solid State*, Vol. 22, p. 41-114, Elsevier, Amsterdam (1980).
7. K. Heide, W. Holand, H. Golker, K. Seyfarth, B. Muller, R. Sauer, *Thermochim. Acta* **13**, 365 (1975).
8. A. M. Gadalla, *Thermochim. Acta* **95**, 179 (1985).
9. A. K. Galwey and M. E. Brown, *Thermal Decomposition of Ionic Solids*, Elsevier, New York (1999).
10. C-R Li, T. B. Tang, *J. Mater. Sci.* **34**, 3467 (1999).
11. K. H. Van Heek, H. Juntgen, *Ber. Bunsenges. Phys. Chem.* **72**, 1223 (1968).
12. S. Vyazovkin, C. A. Wight, *Annu. Rev. Phys. Chem.* 48, 125 (1997).
13. S. V. Vyazovkin, A. I. Lesnikovich, *Russ. J. Phys. Chem.* **62**, 1535 (1988).
14. See appendix A.
15. LiH has a cubic structure with a lattice parameter of $a = 4.083 \text{ \AA}$ and a unit cell volume of 68.1 \AA^3 . LiOH has a tetragonal structure with lattice parameters of $a = 3.553 \text{ \AA}$, $c = 4.348 \text{ \AA}$ and a unit cell volume of 54.9 \AA^3 . Li₂O has a cubic lattice structure with a lattice parameter of $a = 4.611 \text{ \AA}$ and a unit cell volume of 98.1 \AA^3 .
16. HSC, Outokumpu Research Oy, Finland.
17. J. F. McLaughlin, S. S. Cristy, *Composition of Corrosion Films on Lithium Hydride Surfaces After Exposure to Air*, Oak Ridge Y-12 Plant, 1974.

18. J. M. McIntyre, H. M. Smith, American Chemical Society Paper Abstract for the S.E. and S.W. Regional Meeting, December 2-4, 1970, p. 174.

19. H. Lüth, *Solid Surfaces, Interfaces and Thin Films* (Springer, Berlin, 2001).

APPENDIX A

For thin LiOH films grown on LiH in high moisture conditions (H_2O partial pressure on the order of a few hundred Pa or more), the average film growth thickness, x , as a function of time, t can be approximated by Fick's law:

$$J = -D \frac{\Delta C}{\Delta x} \approx -D \frac{C_{surface}}{x} \quad (I)$$

Here J is the flux of H_2O at the LiH surface in units of $molecules.m^{-2}.s^{-1}$, D is the diffusion coefficient of H_2O in the LiOH layer in units of $m^2.s^{-1}$ and $C_{surface}$ is the H_2O concentration at the LiOH/vacuum interface in units of $molecules.m^{-3}$.

But

$$\frac{dx}{dt} = -\frac{J}{C_{in\ solid}} \quad (II)$$

In equation (II), $C_{in\ solid}$ is the concentration of OH^- in the LiOH corrosion layer in units of $molecules.m^{-3}$.

From (I) and (II):

$$\frac{dx}{dt} = D \frac{C_{surface}}{C_{in\ solid}} \frac{1}{x} \quad (III)$$

Or:

$$x^2 = 2 \frac{C_{surface}}{C_{in\ solid}} Dt + A \quad (IV)$$

In equation (IV), A is some initial value of x^2 at $t = 0$ which can be set to 0 in our case. Taking the square root on both sides of equation (IV) yields:

$$x = \sqrt{2 \left[D \left(\frac{C_{surface}}{C_{in\ solid}} \right) \right] t} \quad (V)$$

Here are some approximated values:

$$C_{in\ solid} = \frac{\rho_{LiOH}}{m_{LiOH}} = \frac{1450(kg.m^{-3})}{4 \times 10^{-26}(kg.molecule^{-1})} = 3.63 \times 10^{28} (molecules.m^{-3})$$

From unpublished work $D \left(\frac{C_{surface}}{C_{in\ solid}} \right)$ is on the order of $5 \times 10^{-16} m^2.s^{-1}$ for moisture exposure at room temperature with a 18-30% relative humidity.

FIGURE CAPTIONS

Fig. 1: AFM image of the surface roughness measured on pressed polycrystalline LiH. The top portion of this figure shows a line scan across the surface.

Fig. 2: SEM images of LiOH corrosion layer grown on different facets of pressed polycrystalline LiH after 15 minutes of air exposure at 30% relative humidity (a through d). Larger nanometer-scale grains observed by SEM on some facets of pressed polycrystalline LiH after exposure to room air for 40 minutes (e and f).

Fig. 3: Occasional spallations, blisters and cracks were observed in the morphology of the LiOH corrosion layer grown on polycrystalline LiH after TPR heating up to 550 K.

Fig. 4: (a) TPR spectrum of a fresh salt sample at a heating rate of 0.0015K/s with accompanying cartoons illustrating the ongoing reactions (top) and a blown-up portion of the same spectrum in the lower temperature region (inset); (b) TPR spectrum of bulk LiOH powder decomposition at a heating rate of 0.002 K/s.

Fig. 5: The diffusion of OH⁻ through Li₂O. At no point is water realized within this diffusive system. (a) An H⁺ ion can be seen to hop between successive O₂⁻ ions with a transition state shown in (b). At the Li₂O/LiH interface the two oppositely charged hydrogen ions combine to

generate hydrogen gas(c). An oxide ion shift occurs in order to minimize the energy of the subsequent crystalline void (d). The effective result is the diffusion of OH-

Fig. 6: The equivalent H₂ outgassing spectrum of the sample presented in Fig. 4 can be divided into two subcomponents labeled D3 and R3.

Fig. 7: TPR spectra of total equivalent H₂ release from (a) fresh salt at $\beta = 0.0005$ K/s, (b) baked salt at $\beta = 0.005$ K/s, (c) fresh salt at $\beta = 0.025$ K/s, and (d) baked salt at $\beta = 0.025$ K/s.

Fig. 8: The plots of $\int_0^{\alpha} \ln\left(\frac{d\alpha}{dt}\right) d\alpha$ vs. $\int_0^{\alpha} \frac{d\alpha}{T}$ for (a) fresh salt and (b) baked salt at α value of 0.3, 0.5, and 0.7.

Fig. 9: Activation energy vs. α plots for outgassing from each type of salt studied.

Fig. 10: A plot of the activation energy barrier for outgassing vs. the equivalent LiOH decomposition thickness for fresh salt.

Fig. 11: Comparison between experimental isothermal hydrogen outgassing and isoconversion kinetic prediction for stored/fresh salt at 343 K (a) and annealed/baked salt at 348.7 K (b), 330.1 K (c) and 315.5 K (d).

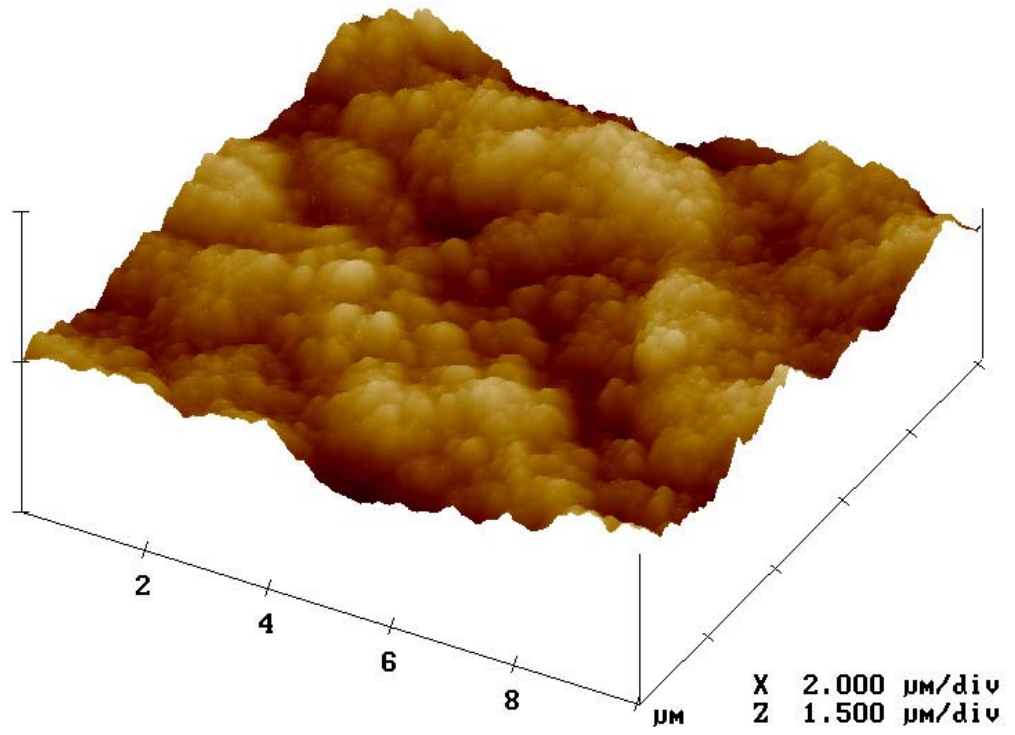
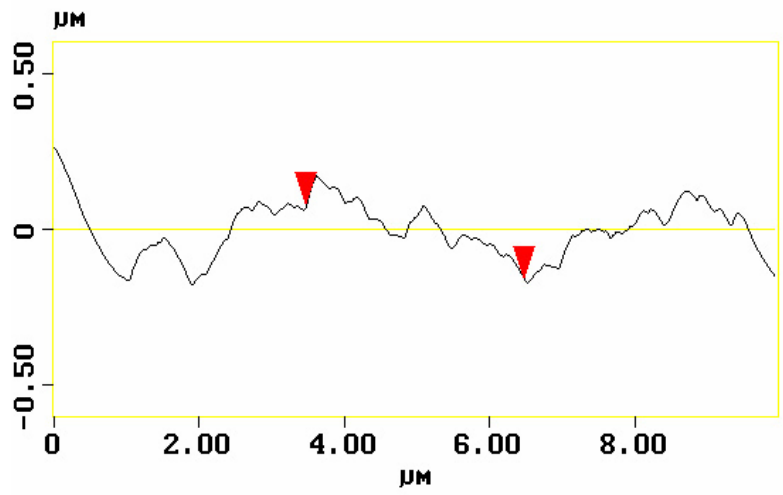


Fig. 1

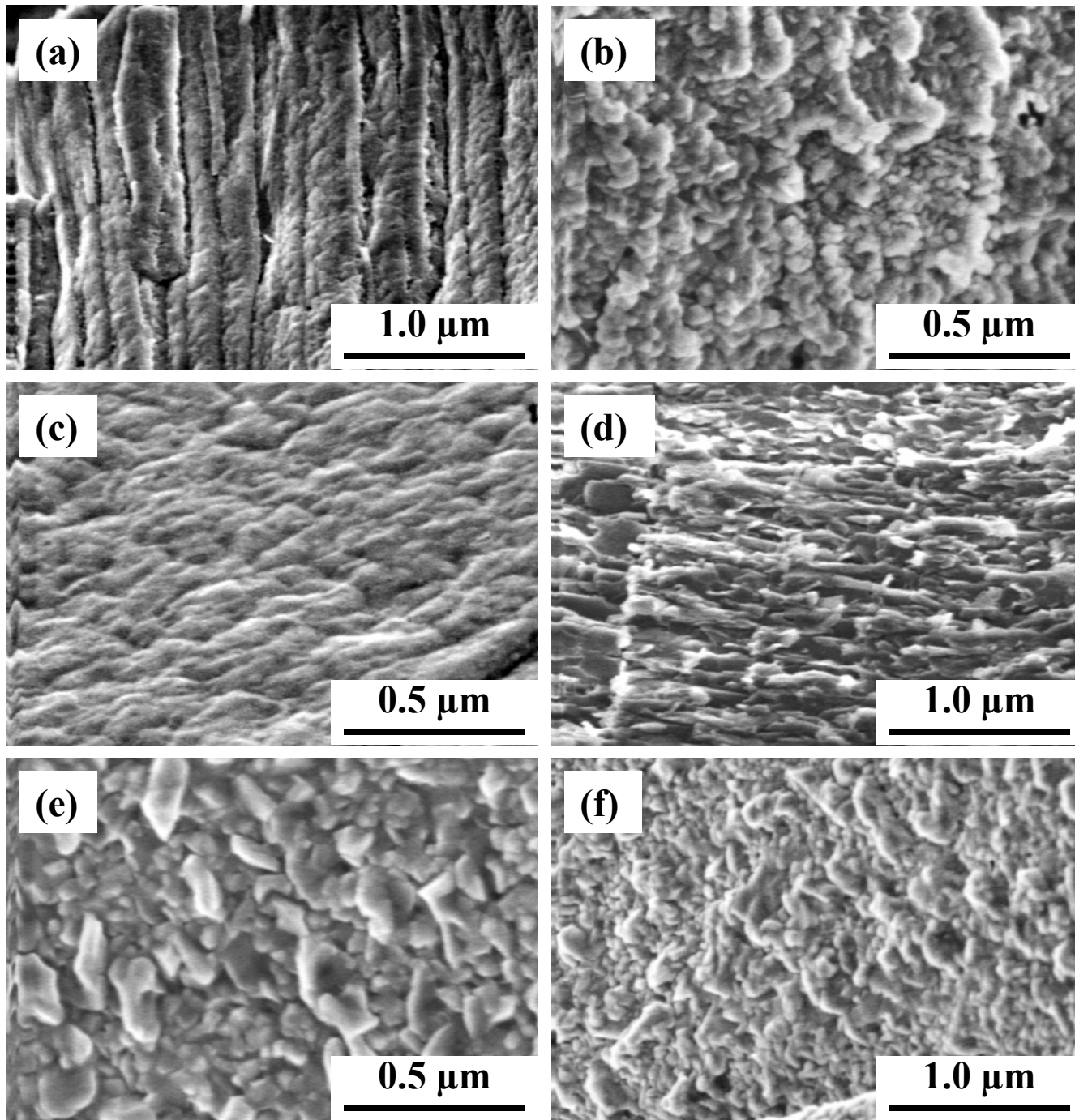


Fig. 2

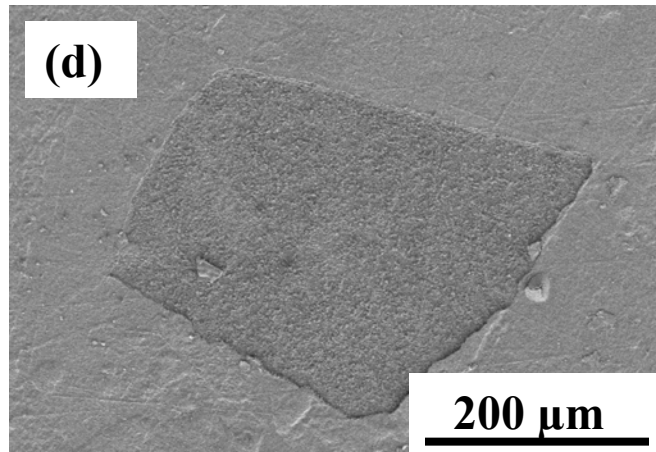
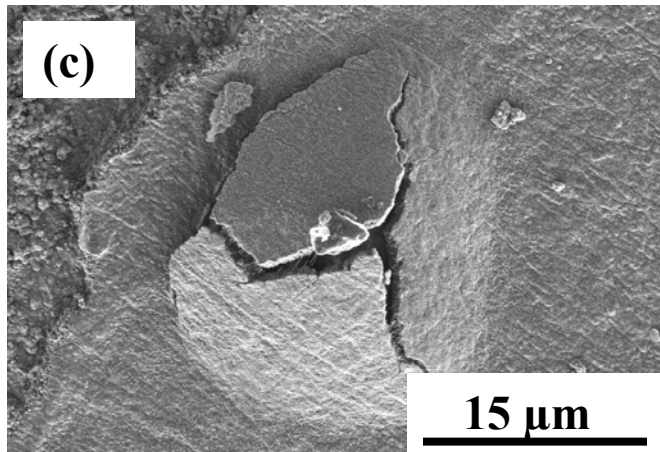
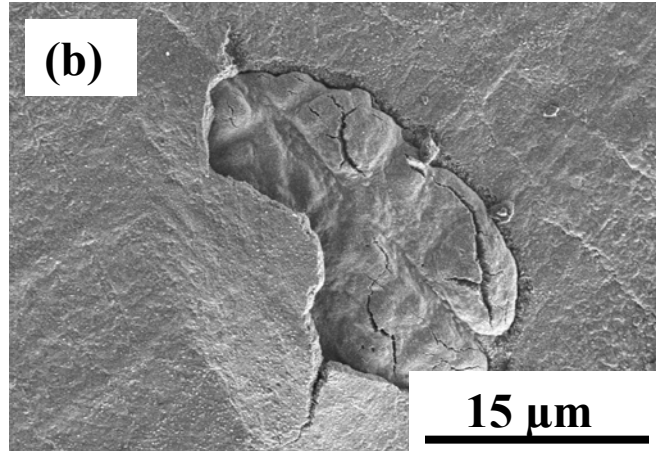
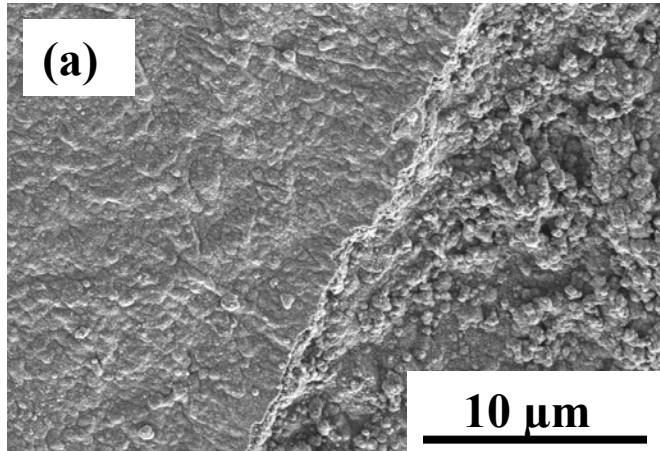


Fig. 3

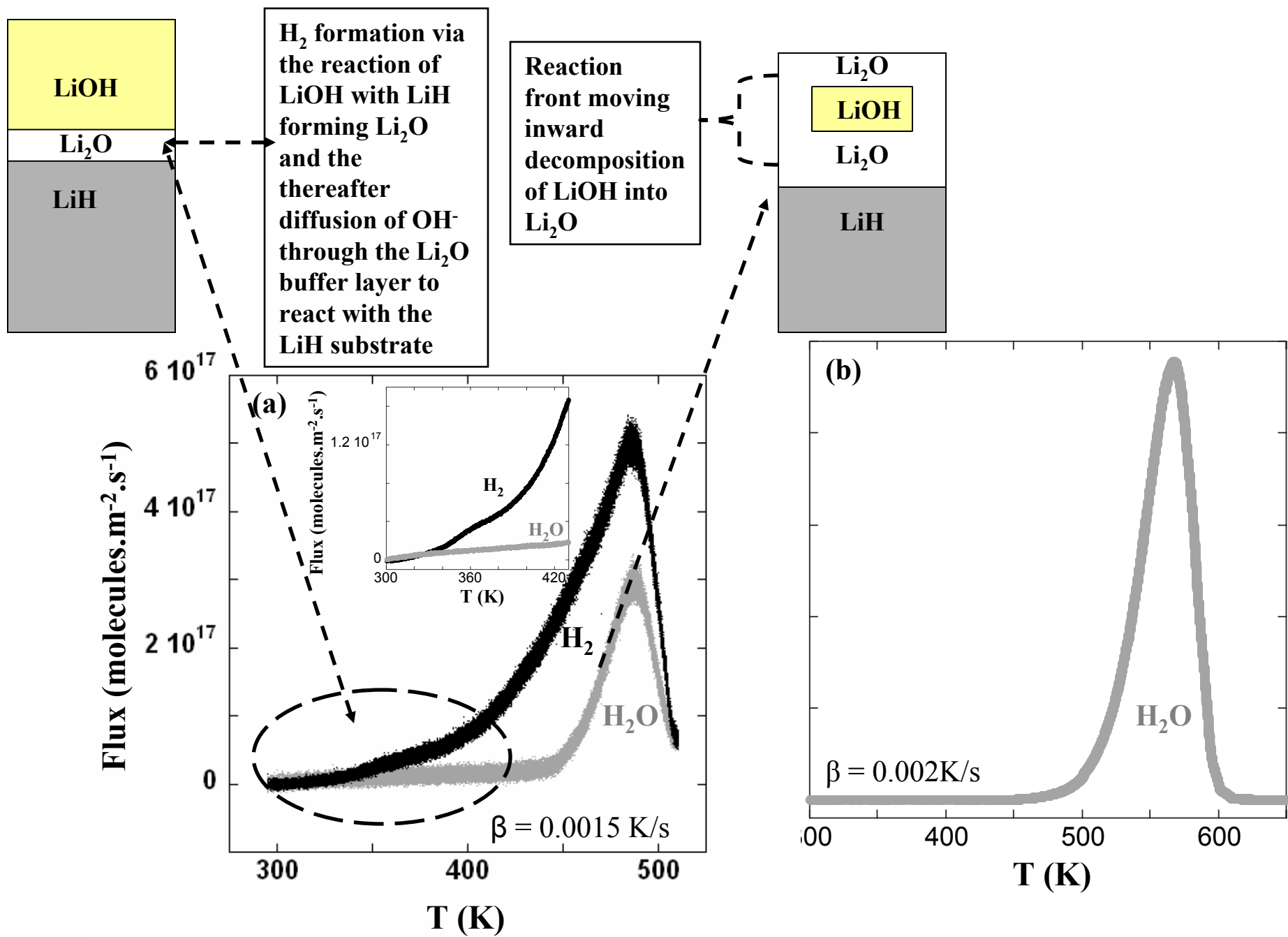


Fig. 4

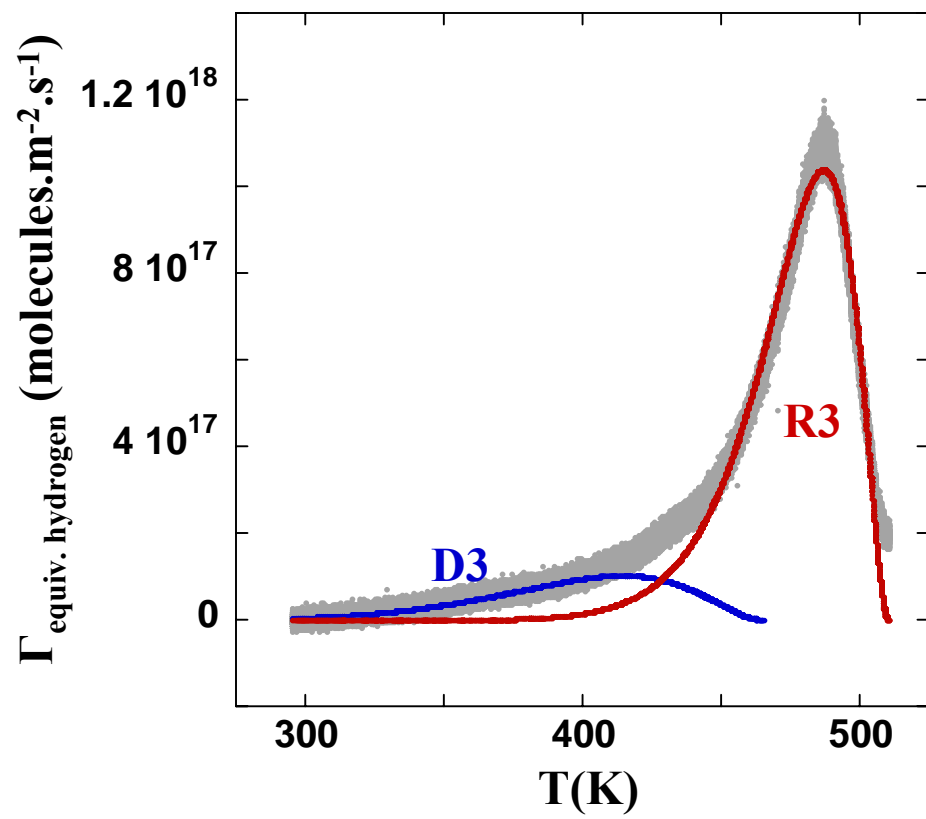


Fig. 6

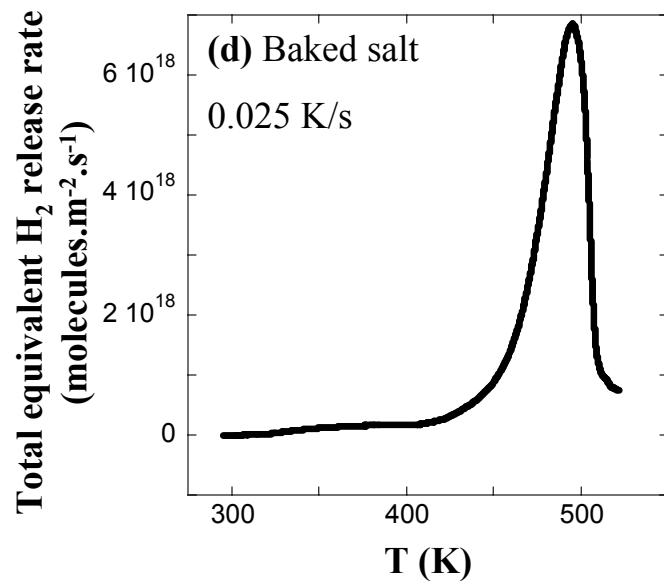
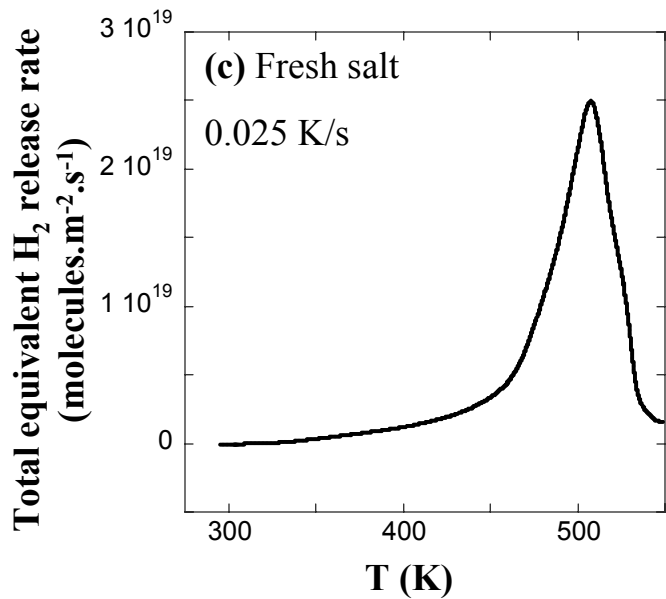
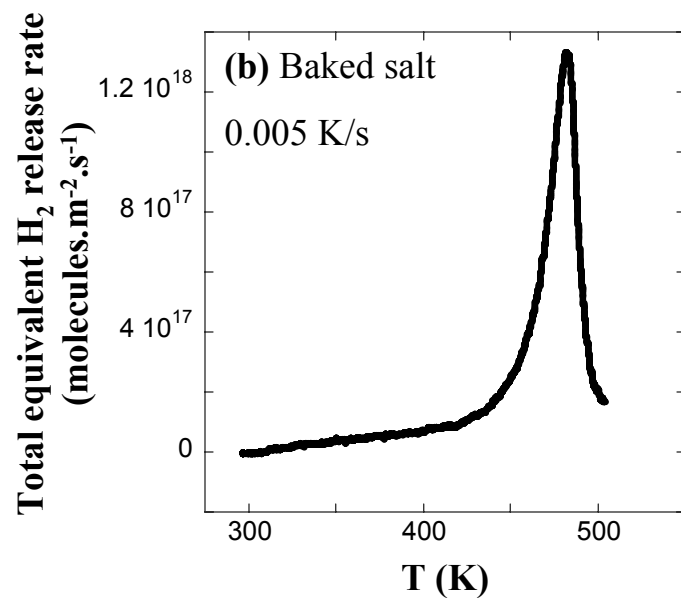
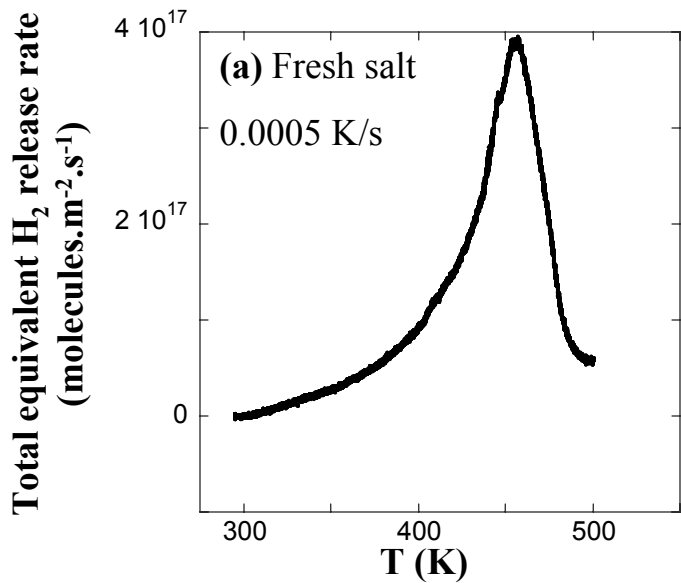


Fig. 7

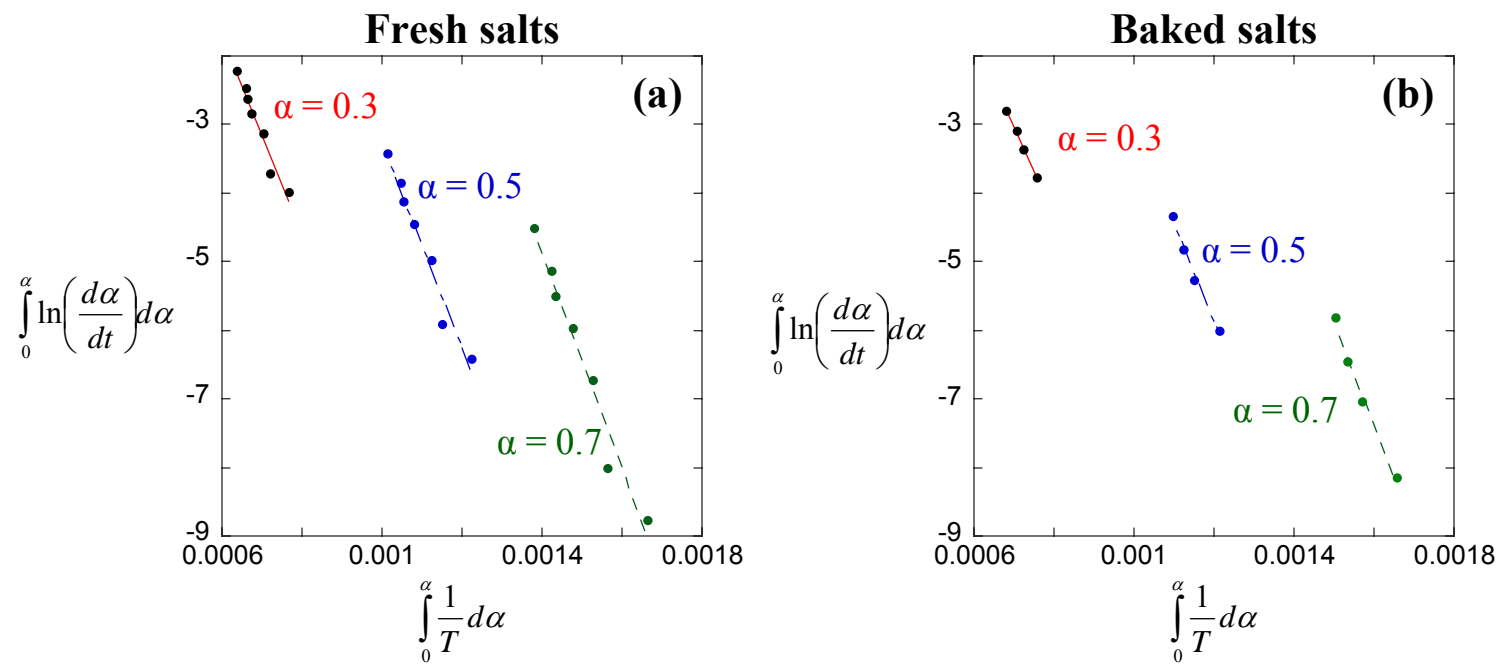


Fig. 8

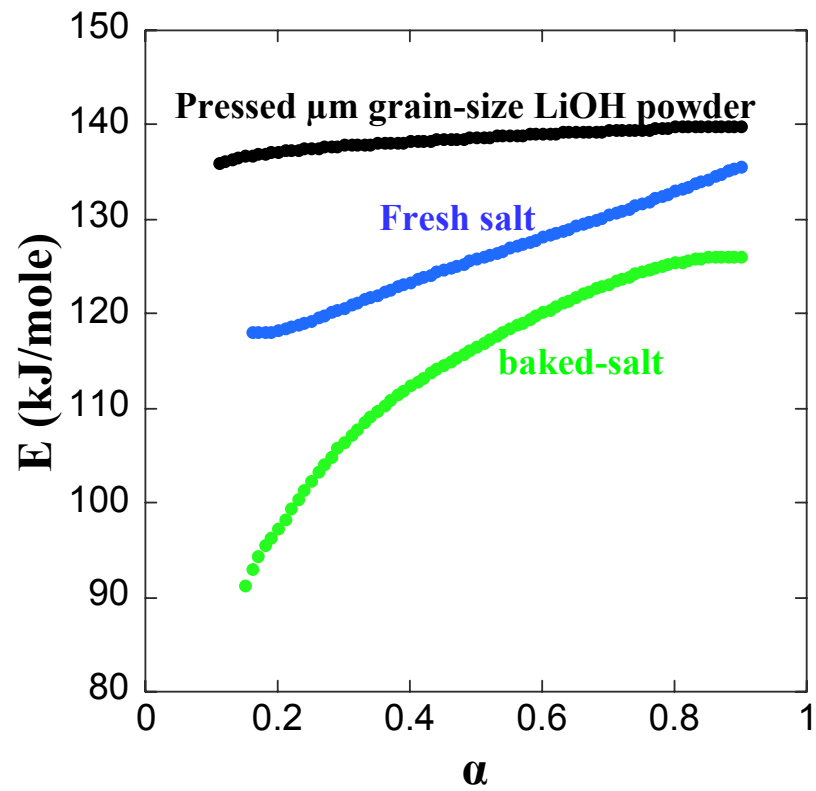


Fig. 9

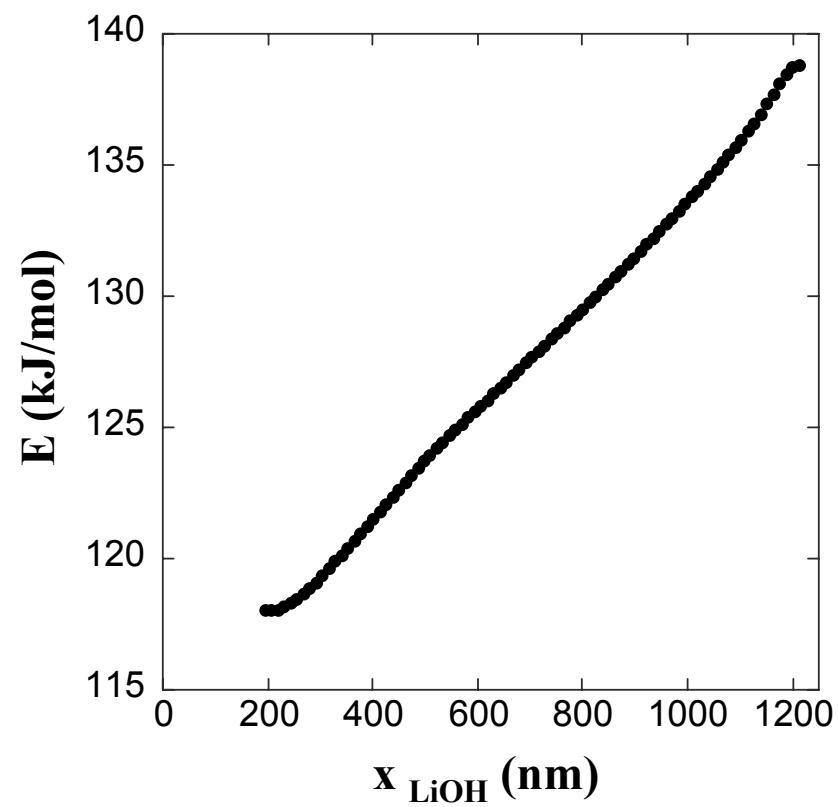


Fig. 10

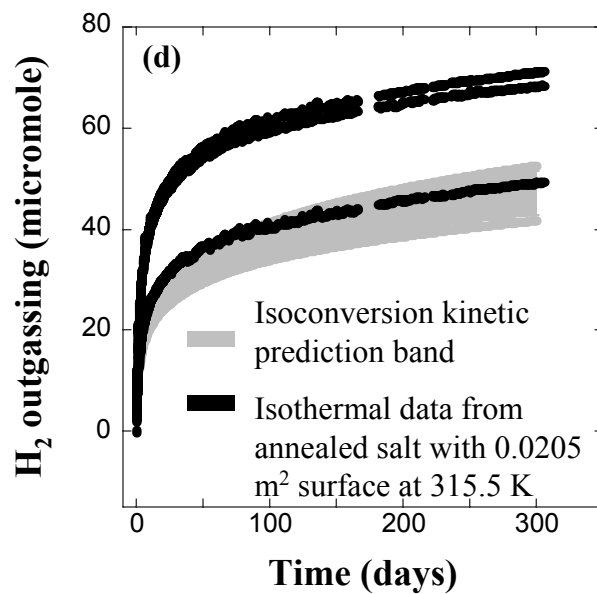
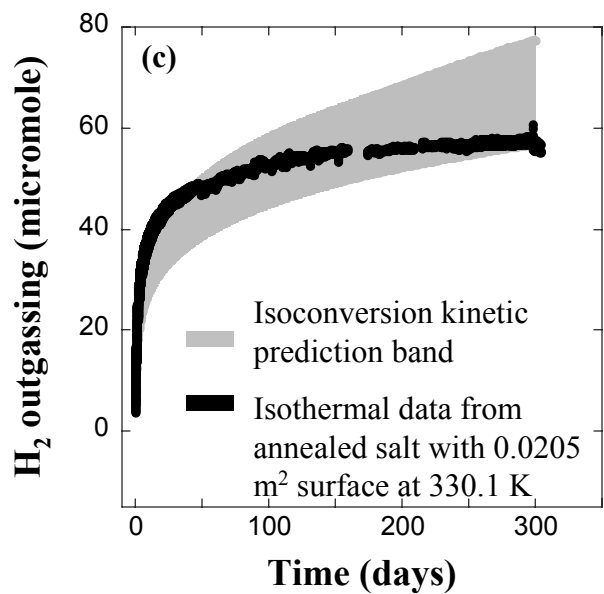
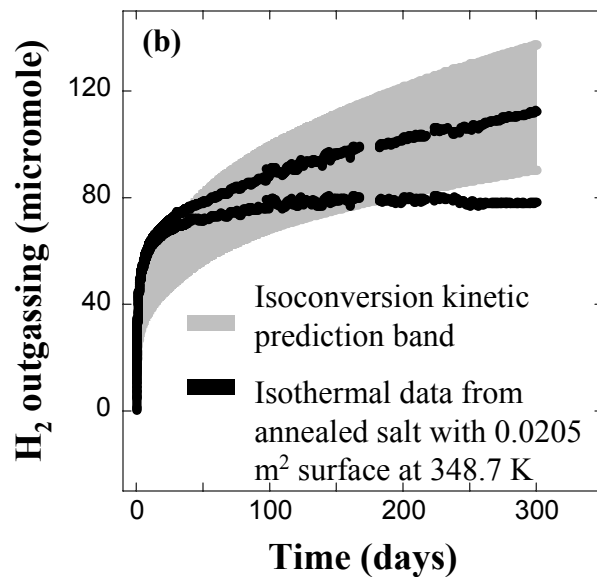
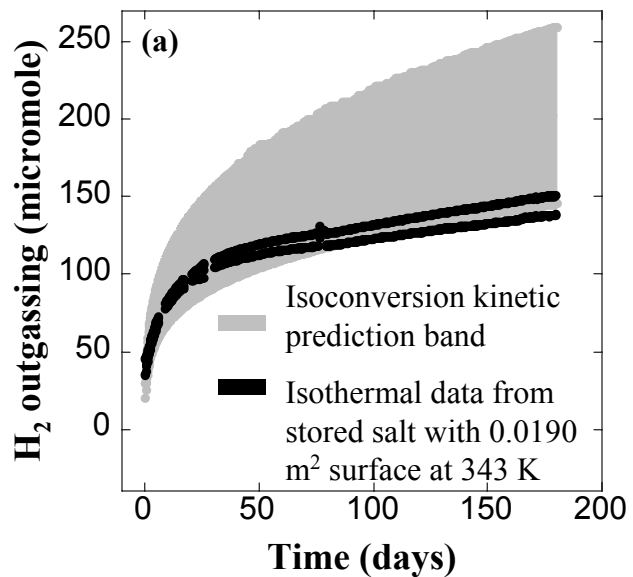


Fig. 11